Cancer Research

Hypoxic Signaling and the Cellular Redox Tumor Environment Determine Sensitivity to MTH1 Inhibition

Lars Bräutigam[1], Linda Pudelko[1], Ann-Sofie Jemth[1], Helge Gad[1], Mohit Narwal[2], Robert Gustafsson[2], Stella Karsten[1], Jordi Carreras Puigvert[1], Evert Homan[1], Carsten Berndt[3], Ulrika Warpman Berglund[1], Pål Stenmark[2], and Thomas Helleday[1]

Abstract

Cancer cells are commonly in a state of redox imbalance that drives their growth and survival. To compensate for oxidative stress induced by the tumor redox environment, cancer cells upregulate specific nononcogenic addiction enzymes, such as MTH1 (NUDT1), which detoxifies oxidized nucleotides. Here, we show that increasing oxidative stress in nonmalignant cells induced their sensitization to the effects of MTH1 inhibition, whereas decreasing oxidative pressure in cancer cells protected against inhibition. Furthermore, we purified zebrafish MTH1 and solved the crystal structure of MTH1 bound to its inhibitor, highlighting the zebrafish as a relevant tool to study MTH1 biology. Delivery of 8-oxo-dGTP and 2-OH-dATP to zebrafish embryos was highly toxic in the absence of MTH1 activity. Moreover, chemically or genetically mimicking activated hypoxia signaling in zebrafish revealed that pathologic upregulation of the HIF1α response, often observed in cancer and linked to poor prognosis, sensitized embryos to MTH1 inhibition. Using a transgenic zebrafish line, in which the cellular redox status can be monitored *in vivo*, we detected an increase in oxidative pressure upon activation of hypoxic signaling. Pretreatment with the antioxidant N-acetyl-L-cysteine protected embryos with activated hypoxia signaling against MTH1 inhibition, suggesting that the aberrant redox environment likely causes sensitization. In summary, MTH1 inhibition may offer a general approach to treat cancers characterized by deregulated hypoxia signaling or redox imbalance. *Cancer Res; 76(8); 2366–75. ©2016 AACR.*

Introduction

Redox signaling, the signal transduction through oxidation and reduction, is a fundamental process in cellular physiology and pathology (1, 2). Since early observations that many cancer cells are suffering from oxidative stress (3), it has been well established that the redox environment of malignant cells is unique and distinct from healthy counterparts, indeed being essential for cancer to manifest, grow, and spread (4). Moreover, the oncogenic redox system acts in concert with the cellular hypoxia-VHL-HIF axis, adjusting the cellular metabolism to meet the specific demands of the cancer cell, and to regulate tumor growth, angiogenesis, and metastasis (5, 6).

However, the oncogenic redox environment comes with a cost because it imposes high oxidative pressure on the cancer cell and requires upregulation of antioxidant systems and other nononcogenic addiction enzymes (7). Therefore, the tightly balanced oncogenic redox system is presenting an attractive target for novel anticancer therapies (8–10). However, as solely increasing oxidative stress to induce cancer cell death seems to be insufficient (11), other strategies to target the cancer-specific redox environment might be more effective.

The free nucleotide pool of cancer cells is especially vulnerable to oxidative damage (12) and requires efficient protection as oxidized nucleotides can lead to mispairing, mutations, and cell death (13–15). 8-oxo-dGTP is one of the most prevalently oxidized nucleotides and can induce G:C to T:A and *vice versa* transversions if not detoxified. The human mutT homologue (MTH1) efficiently sanitizes the cellular dNTP pool and converts, amongst others, 8-oxo-dGTP and 2-OH-dATP into their respective monophosphates (16). MTH1 has been extensively described as an nononcogenic addiction enzyme (17, 18), and we have recently identified MTH1 inhibitors as promising anticancer agents (19), as we were able to show that siRNA-mediated knockdown of MTH1 induces DNA damage and cancer cell death in *vitro* and *in vivo*. In addition, we developed small-molecule inhibitors, including TH588, that selectively target MTH1 and lead to cell death of different cancer cell lines as well as show promising *in vivo* activity (19, 20). Here, we describe how artificial changes of the cellular redox system in *vitro* and *in vivo*, and challenges with oxidized nucleotides influence sensitivity to MTH1 inhibition. Furthermore, we provide evidence that activation of the VHL-HIF axis,

[1]Science for Life Laboratory, Division of Translational Medicine and Chemical Biology, Department of Medical Biochemistry and Biophysics, Karolinska Institutet, Stockholm, Sweden. [2]Department of Biochemistry and Biophysics, Stockholm University, Stockholm, Sweden. [3]Department of Neurology, Medical Faculty, Heinrich-Heine-University Düsseldorf, Life Science Center, Düsseldorf, Germany.

Note: Supplementary data for this article are available at Cancer Research Online (http://cancerres.aacrjournals.org/).

Corresponding Authors: Lars Bräutigam, Division of Translational Medicine and Chemical Biology, Department of Medical Biochemistry and Biophysics, Karolinska Institutet, Stockholm S-17121, Sweden. Phone: 070-759-1481; Fax: 46-8-52481425; E-mail: lars.brautigam@scilifelab.se; and Thomas Helleday, thomas.helleday@scilifelab.se

doi: 10.1158/0008-5472.CAN-15-2380

AACR

a common phenomenon of many cancers, sensitizes to inhibition of MTH1 enzymatic activity, likely due to an increase of the oxidative burden.

Materials and Methods

Chemicals

N-acetyl-L-cysteine (Sigma) was dissolved to 100 mmol/L in HEPES buffer for cell experiments or PBS for zebrafish experiments, pH was adjusted to 7.4 and the solution used directly. $KBrO_3$ (Sigma) was dissolved in HEPES to 100 mmol/L and used directly. DMOG (dimethyloxalylglycine; Sigma) was dissolved in water to 100 mmol/L, stored at −20°C in aliquots, and discarded after one freeze-thaw cycle. PEG-catalase and L-Buthionine-sulfoximine (Sigma) were dissolved in HBSS. Synthesis and chemical properties of the MTH1 inhibitor TH588 have been described before (19). It was dissolved in DMSO to 10 mmol/L for celluar or 100 mmol/L for crystallographic studies.

RNA isolation, reverse transcription, and quantitative PCR

RNA was isolated from a pool of 30 zebrafish embryos using the RNA isolation Kit (Thermofisher) and 0.5 μg RNA was used for DNA-free cDNA synthesis (Maxima cDNA Kit, Thermo Fisher). qRT-PCR was performed on a Rotorgene (Qiagen) using the Luminaris Color HiGreen Sybr Green mix (Thermo Fisher). The $\Delta\Delta C_t$ method was used for quantification and comparison, and β actin was used as verified housekeeping gene (21). Primers always span an exon/intron junction for RNA specificity; sequences see Supplementary Table S4.

Cloning, protein purification, and biochemical analysis

Zebrafish MTH1 (NM_ 213418) was amplified from zebrafish cDNA (primer see Supplementary Table S4). ZfMTH1 protein was expressed in Rosetta (DE3; Millipore) by induction with 1 mmol/L IPTG at an OD_{600} of 0.8 and further growth at 17°C for 19 hours. Bacteria were harvested by centrifugation and lysed in IMAC buffer [50 mmol/L HEPES, pH 7.5, 500 mmol/L NaCl, 10 % (v/v) glycerol, 10 mmol/L imidazole] using high-pressure homogenization followed by centrifugation and filtration. Lysate was treated with Benzonase (0.1 μL/mL) and protease inhibitor cocktail (Roche) and 0.5 mmol/L TCEP (Sigma) was added. His-tagged zfMTH1 was purified on a His TrapFF column (GE Healthcare), washed with Buffer A (50 mmol/L HEPES buffer, pH 7.5, 500 mmol/L NaCl, 10 % glycerol, and 0.5 mmol/L TCEP), fortified with 50 mmol/L Imidazol, followed by elution of the protein with buffer A fortified with 300 mmol/L Imidazol. ZfMTH1 containing fractions were pooled, loaded on a Superdex 200 16/600 column (GE Healthcare), and separated using buffer B (20 mmol/L HEPES, pH 7.5, 500 mmol/L NaCl, 5 % glycerol and 0.5 mmol/L TCEP). Fractions containing zfMTH1 was pooled and purity was analyzed on SDS-PAGE. Protein concentration was determined using a calculated extinction coefficient of 24,980 $M^{-1}cm^{-1}$. The IC_{50} value of zfMTH1 and hMTH1 using 5 nmol/L enzyme was determined as described previously (19). Kinetic analysis of zfMTH1 was performed by determining initial rates of substrate hydrolysis at varying concentrations of dGTP (0–400 μmol/L), 8-oxo-dGTP (0–100 μmol/L) and 2-OH-dATP (0–100 μmol/L) in MTH1 reaction buffer (100 mmol/L Tris Acetate, pH 7.5, 40 mmol/L NaCl, 10 mmol/L MgAcetate, 1 mmol/L DTT). For dGTP hydrolysis 1.5 nmol/L zfMTH1 was used and for 8-oxo-dGTP and 2-OH-dATP hydrolysis 0.3 nmol/L was used. Formed PPi was detected using the PPiLight Inorganic Pyrophosphate Assay from Lonza. The Michaelis Menten equation was used to calculate kinetic parameters using nonlinear regression analysis and the GraphPad Prism software.

Crystallographic studies

ZfMTH1 protein for crystallographic studies was expressed in BL21 (DE3; Novagen) mainly as described above; however, the washing and elution buffer contained only 300 mmol/L NaCl and 5 % glycerol by induction with 0.5 mmol/L IPTG at an OD_{600} of 1.0 in Terrific Broth media and further growth at 18°C for 20 hours. Bacteria were harvested by centrifugation and lysed in Lysis buffer [100 mmol/L HEPES, pH 8.0, 500 mmol/L NaCl, 10 % (v/v) glycerol, 0.5 mmol/L TCEP] after treatment with lysozyme, 5 mmol/L $MgSO_4$, DNAse, and protease inhibitor cocktail (Roche) using high-pressure homogenization followed by centrifugation. His-tagged zfMTH1 was purified on gravity flow column (Econo-Pac Chromatography column, Bio-Rad) after incubation with Ni-NTA (1.5 mL/50 mL cleared lysate) and 10 mmol/L Imidazole, washed with Buffer A (20 mmol/L HEPES buffer, pH 7.5, 500 mmol/L NaCl, 10 % glycerol, and 0.5 mmol/L TCEP) fortified with 10 mmol/L Imidazole followed by elution of the protein with Buffer A fortified with 500 mmol/L Imidazole. ZfMTH1 containing fractions were pooled, loaded on a Superdex 75 16/60 column (GE Healthcare), and separated using Buffer B (20 mmol/L HEPES, pH 7.5, 300 mmol/L NaCl, 10% glycerol, and 0.5 mmol/L TCEP). Fractions containing zfMTH1 were pooled and purity was analyzed on SDS-PAGE. Protein was concentrated using Vivaspin 20 (Sartorious Stedim), 10 kDa MWCO at 4,800 rcf at 4°C. Concentration was determined using a calculated extinction coefficient of 24,980 $M^{-1}cm^{-1}$. Details for the crystallization can be found in the Supplementary Methods.

Zebrafish maintenance, injection, and exposure

Zebrafish were raised and staged according to standard protocols. Zebrafish with mutated VHL (*vhl*^{hu2117}) has been described before (22) and obtained from ZIRC (www.zebrafish.org). Homozygous knockouts can be identified morphologically; heterozygous cannot be distinguished from wild-types. A detailed description of how the ZebROS transgenic line was established and imaged can be found in the Supplementary Methods. Embryos were exposed to chemicals in 12-well plates with 20 embryos and 1 mL E3 medium per well. Capped zfGpx1 mRNA was synthesized using the mMessage/Machine Kit (Ambion). For injection experiments, 8-oxo-dGTP, 2-OH-dATP (Jena Biosciences), and capped mRNA (50 pg/embryo) were mixed with injection buffer (9 μmol/L spermine, 0.21 μmol/L spermidine, and 0.3 % phenol red) and injected into 1-cell stage zebrafish embryos. In all experiments, embryos with cardiac arrest were regarded as dead. All experiments were performed in accordance to the local ethical guidelines (N207/14).

Cell culturing and cellular assays

BJ-hTERT cells have been obtained from Dr. William Hahn (Dana-Farber Cancer Institute, Boston, MA) during the last 5 years, all other cell lines from ATCC during the last 3 years. All cell lines have been authenticated by the providers and were

cultivated in conditions specified by the provider. For survival assays, cells were seeded in 96-well plates and exposed to MTH1 inhibitors 24 hours after seeding. Three days after exposure, survival of the subconfluent culture was determined using the resazurin assay as described before (19). In some experiments, cells were exposed to 1 mmol/L $KBrO_3$ for 15 minutes followed by three washes with PBS. The modified comet assay with OGG1 detecting 8-oxodG lesions in DNA was done as described before (19). Cellular glutathione levels were determined with the GSH -Glo Kit (Promega) following the manufacturer's instructions and normalized to total cellular protein. Cells expressing shRNA constructs to knock down VHL (5′-GATCTGGAAGACCACC-CAAAT-3′) were produced with a lentiviral system following standard procedures.

Crystallization

TH588 and TCEP (final concentration of 2 mmol/L) were added to zfMTH1 before crystallization and mixture was incubated on ice for 30 minutes. Proteases (1:400 ratio each of trypsin, α-chymotrypsin, pepsin, papain, proteinase K, and subtilisin to zfMTH1) were added just before the crystallization. Sitting drop vapor diffusion at 20°C was performed, and MTH1 (54 mg/mL) was mixed with reservoir solution (28% PEG10K, 100 mmol/L sodium acetate, pH 4.0, and 200 mmol/L Li_2SO_4) in a 3:1 ratio. Diffraction quality crystals appeared after about 2 days, and were subsequently flash frozen in liquid nitrogen without cryo-protectant. Data collection was performed beamline 14.1 at BESSY, at 100 K. Data reduction and processing were carried out, using XDS (23), programs from the CCP4 suite (Collaborative Computational Project 4, 1994), and Phenix (24). Relevant statistics can be found in Supplementary Table S2.

The structure was solved via molecular replacement, using the previously solved human MTH1 structure as search model (PDB code: 3ZR1;25). A few cycles of refinement in Refmac5 (26) and Phenix (24), interspersed with manual building in Coot (27), were needed to complete the model. Water molecules were automatically placed in the maps, using a F_O-F_C Fourier difference map cutoff of 3σ, and subsequently validated to ensure correct positioning. The final protein model contains residues 3–156. RMSD value of C-alphas between crystal structures of human and zfMTH1 with TH588 was calculated using online server DaliLite. The data show a strong (44%) off-origin patterson peak characteristic of pseudo translational symmetry. However, the electron density, data quality, and the quality of the resulting structure are of very high quality (Supplementary Table S2; Supplementary Fig. S7). All structure figures were prepared using PyMOL. Ramachandran statistics were generated using MolProbity. The structure has been deposited in the protein data bank with accession code 5HZX.

Generation and imaging of ZebROS transgenic embryos

Constructs for measuring the mitochondrial glutathione pool were a kind gift of Tobias Dick (DKFZ, Heidelberg, Germany). The sequence encoding the redox sensor has been amplified and equipped with Gateway cloning attachment sites by PCR using the primer 5′- GGGGACAAGTTTGTACAAAAAAGCAGGCTT-CATGGCCTCCACTCGTGTCCTC -3′ and 5′- GGGGACCACTTTG-TACAAGAAAGCTGGGTCCTATTCCACCTCTTTCAAAAG -3′. The amplified sequence was cloned into the pDONOR vector and subsequently in a destination vector containing Tol2 sites and a cmlc2 marker (28). The construct was injected together with capped mRNA encoding for Tol2 recombinase into one cell stage TL embryos. The founder generation (F0) was raised to adulthood, screened for germline transmission, and inbred three times to ensure stable genomic integration. Imaging of the redox sensor was done as described before (29). Briefly, embryos were transferred into a black, clear bottom 96-well imaging plate (corning) with one embryo per well. After exposure to chemicals, embryos excited sequentially with 405 and 492 nm and absorption was detected at 510 nm. Oxidative state of the cell is expressed as absorbance ratio 405/492 nm.

Documentation and statistical analysis

Pictures of zebrafish were taken with a Leica MZ16 microscope equipped with a Leica DCF3000FX camera. Images were processed with Gimp (www.gimp.org) without obstructing any original data. Data are expressed as mean ± SD. Statistical significance was calculated using the two-tailed Student *t* test. *, $P < 0.05$; **, $P < 0.01$; ***, $P < 0.005$.

Results

Lost redox homeostasis sensitizes cells to MTH1 inhibition

We have previously demonstrated that sensitivity of cancer cells due to loss-of-functional MTH1 is correlated with incorporation of 8-oxoG into DNA (19, 20). Because we observed that elevated levels of total glutathione, as found for example, in cancer cells, correlate with an increased sensitivity to MTH1 inhibition, we investigated whether the redox environment of cells determines sensitivity to MTH1 inhibition (see Supplementary Table S1). Therefore, we exposed immortalized non-transformed fibroblasts (BJ hTERT) to the non-alkylating oxidation agent $KBrO_3$ before treatment with the MTH1 inhibitor TH588. As previously reported, TH588 alone was nontoxic to BJ hTERT cells; however, pretreatment with $KBrO_3$ sensitized cells to TH588 by 20% ± 4% in a wide concentration range of 39 nmol/L to 10 μmol/L of the inhibitor (see Fig. 1A). Besides, we also increased the cellular redox pressure by blocking glutathione *de novo* synthesis in U2OS osteosarcoma and U343 asctrocytoma cells using L-Buthionine-sulfoximine (BSO). Exposure to 50 μmol/L BSO for 24 hours reduced total glutathione levels by 95 % and sensitized both cell lines significantly to MTH1 inhibition (U2OS 62 ± 7,5 % vs. 72 ± 4 %, $P = 0{,}0004$ and U343 74 ± 9 % vs. 86 ± 2 %, $P = 0{,}0003$ survival for BSO or controls respectively; see Supplementary Fig. S1). In line with this, we were able to reduce sensitivity of cancer cells to MTH1 inhibitors by an often used general antioxidant, N-acetyl-L-cysteine (NAC). After pretreatment of U2OS osteosarcoma cells with 4 mmol/L NAC for 2 hours, we observed a slight but significant protection against TH588 ($P = 0.027$, see Fig. 1B). This protective effect of NAC correlated with a reduced incorporation of 8-oxoG into DNA, as shown by a modified comet assay in which the enzymatic activity of OGG1 is used to monitor 8-oxodG lesions (see Fig. 1C and D). Next, we wanted to investigate whether only thiol-related antioxidants or also thiol-independent antioxidants are able to protect cancer cells against MTH1 inhibition. Therefore, U2OS and A549 cells were pretreated with PEG-catalase. As expected, pretreatment with PEG-catalase itself had no effect on the total glutathione level or 2GSH/GSSG redox state, but

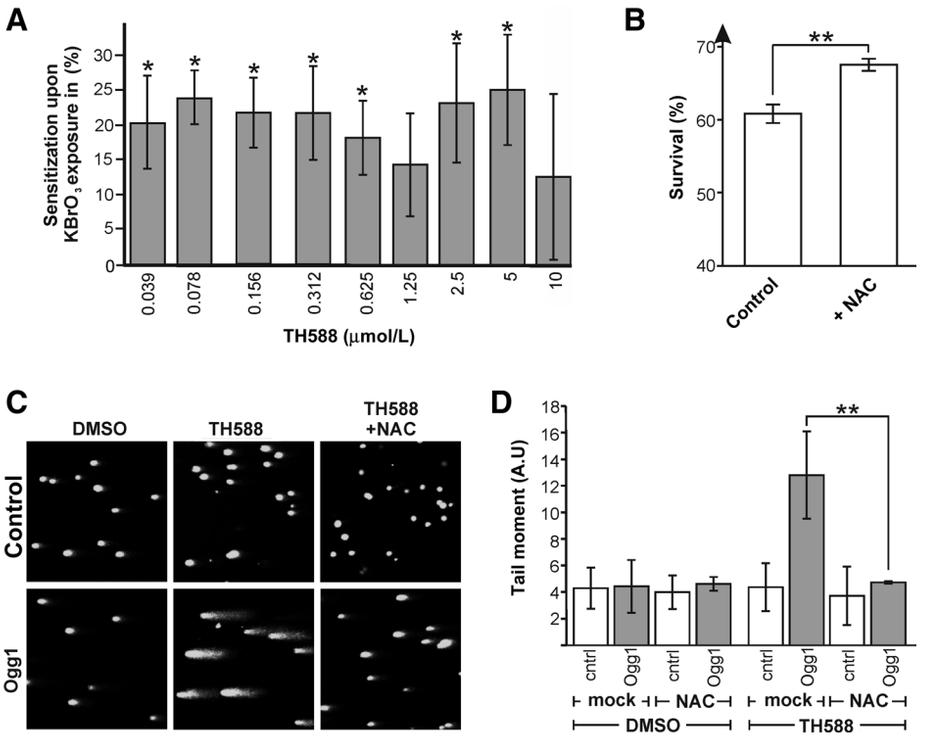

Figure 1.
The cellular redox environment determines sensitivity to MTH1 inhibition. A, Bj hTERT cells (immortalized fibroblasts) pretreated with 1 mmol/L $KBrO_3$ for 15 minutes were sensitized to the MTH1 inhibitor TH588 by 20 ± 4 % ($n = 3$). B, U2OS cells (osteosarcoma) pretreated with 10 mmol/L NAC for 2 hours were protected against the effect of 5 μmol/L TH588 (control 62.3 ± 2.3 % viability, NAC pretreatment 67.4 ± 1.5 %viability; $n = 3$; **, $P = 0.027$). C, modified comet assay revealed that pretreatment of U2OS cells with 10 mmol/L NAC for 2 hours significantly reduced the incorporation of 8-oxo-dGTP into DNA when MTH1 was inhibited. D, quantification of comet assay ($n = 3$; **, $P = 0.022$).

protected cells significantly against TH588 exposure (see Supplementary Fig. S2)

Zebrafish as a model to study MTH1 biology

MTH1 is highly conserved throughout evolution and human and zebrafish MTH1 (zfMTH1) show a 70 % identity on amino acid level (see Supplementary Fig. S3). We cloned, expressed, and purified zfMTH1 (see Supplementary Fig. S4) and found that the MTH1 inhibitor TH588 showed similar affinity to zfMTH1 as to human MTH1 (2.8 ± 0.6 nmol/L and 1.4 ± 0.4 nmol/L, respectively, $n = 3$; see Fig. 2B). To study the interaction more closely, we solved the structure of the zebrafish MTH1 with the inhibitor TH588 bound to a resolution of 1.9 Å (Supplementary Table S2), which revealed a high overall structural similarity (see Fig. 2A). The C-alpha RMSD between human and zebrafish MTH1 is 0.9 Å. The electron density is of good quality and clearly defines TH588 in the active site of MTH1 (Supplementary Fig. S5). Importantly, with critical interactions between ligand features and surrounding residues being the same, our previously developed MTH1 inhibitor TH588[19] binds almost identical, when comparing the human and zebrafish TH588 complexes (see Fig. 2A). Within a 6.0 Å shell of TH588, there are three different amino acids that discriminate human and zebrafish MTH1: Tyr7Leu, Pro118Ala, and Gln142His. The latter two are located at the outer edge and somewhat shielded from TH588 by bulky residues (Phe27 and Trp117), and hence predicted to have little effect on affinity. Whereas, both Leu and Tyr at position 7 are within van der Waals distance to TH588, but the aromatic properties of Tyr7 does not affect the affinity, as TH588 has comparable IC_{50} values for both zebrafish and human MTH1 proteins. In the crystal structure of zebrafish MTH1, the C-terminus of one monomer is in close vicinity of the active site of the neighboring molecule. The carboxyl of Leu156 is 5 Å away from TH588 in the neighboring protein and forms a hydrogen bond to Lys23 of the neighboring molecule and to the sulfate bound close to the inhibitor (Fig. 2A). The crystal contact of the C-terminus (Leu156) of one monomer to the neighboring molecule will not affect the affinity of TH588, as zfMTH1 is present as a monomer in solution. Furthermore, the complex between TH588 and MTH1 is made before the crystal lattice is formed. The largest structural differences between the zebrafish and human MTH1 structures are the positions of the five most C-terminal residues (aa 152–156). Moreover, like hMTH1, zfMTH1 displays highest catalytic efficiency to 2-OH-dATP followed by 8-oxo-dGTP ($2 \times 10^6 \pm 1.4 \times 10^5\ M^{-1}s^{-1}$ and $1.4 \times 1\,0^6 \pm 1.5 \times 10^5\ M^{-1}s^{-1}$, respectively (see Fig. 2C and Supplementary Table S3). We have determined that zebrafish eggs can be exposed to 1.5 μmol/L TH588 without affecting viability or morphology (viable embryos 86.4 ± 14.2 %, $P = 0.125$; $n = 280$). In conclusions, we have established that the inhibitor TH588 is a useful tool to study the biology of MTH1 in zebrafish.

8-oxo-dGTP and 2-OH-dATP are toxic to zebrafish in absence of MTH1 activity

It is generally believed that 8-oxoG in DNA is nontoxic since mice lacking OGG1 or MTH1 survive (30, 31) and replication forks remain intact. Earlier, we demonstrated that MTH1 inhibition is toxic to cancer cells (19), and it is unclear whether this is related by incorporation of 8-oxoG into DNA or if this is explained by incorporation into RNA (32). To unravel whether functional MTH1 is required to detoxify oxidized nucleotides *in vivo*, we microinjected 8-oxo-dGTP and 2-OH-dATP (1.5 nL of a 1.3 mmol/L solution) into zebrafish eggs. Because we inject the deoxy form of the oxidized nucleotides, it is likely to be incorporated into DNA. Injection of 8-oxo-dGTP alone reduced viability

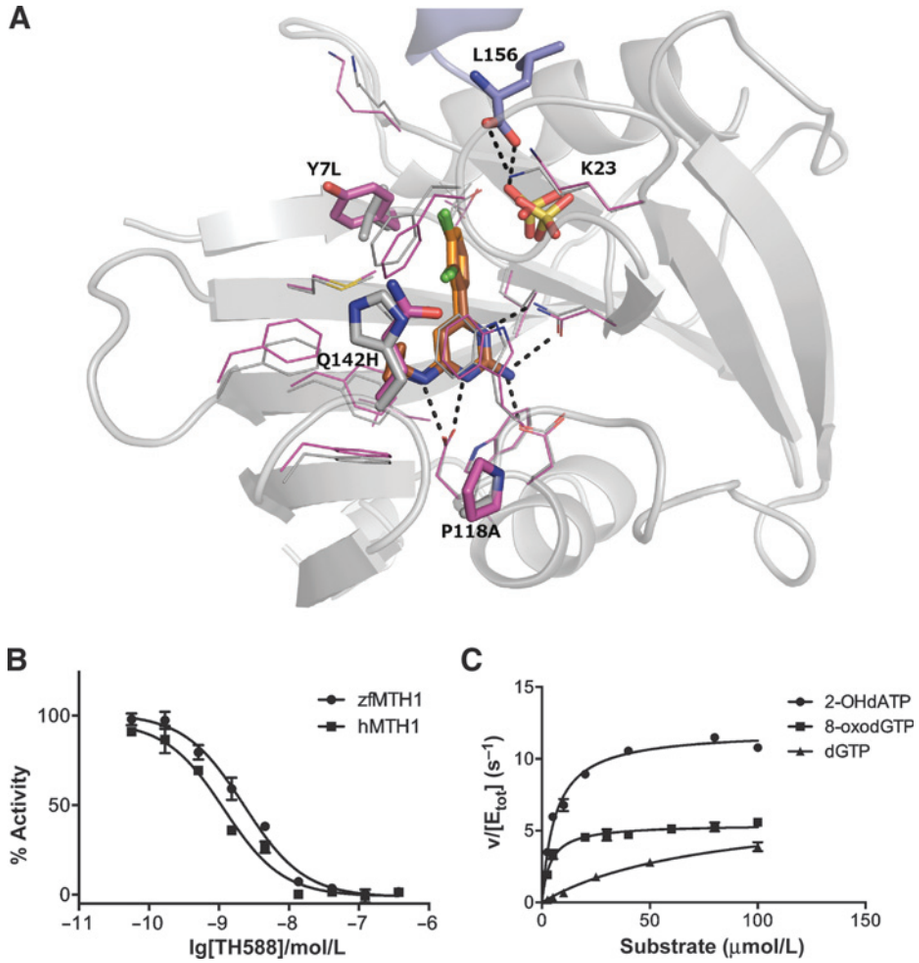

Figure 2.
Structural and biochemical analysis of zfMTH1. A, zebrafish MTH1 crystal structure (gray) in complex with the inhibitor TH588 (orange) overlaid with the crystal structure of human MTH1 (purple) in complex with the inhibitor TH588 (brown). Residues within 6 Å of TH588 are shown as lines and H-bonds are shown as dashed lines (black). Also, residues different from human MTH1 (Tyr7Leu, Pro118Ala, and Gln142His) in the vicinity of TH588 are shown as sticks. Leu156 from the neighboring chain (blue) and bound sulfate are shown as sticks. B, the IC_{50} of TH588 for zfMTH1 was determined to be 2.8 ± 0.6 nmol/L as compared with 1.4 ± 0.4 nmol/L for hMTH1. C, as for hMTH1, 2-OH-dATP and 8-oxo-dGTP are preferred substrates compared with dGTP. Catalytic efficiency (k_{cat}/K_M) of 2-OH-dATP is $2 \times 10^6 \pm 0.14 \times 10^6$ $M^{-1}s^{-1}$ and $1.4 \times 10^6 \pm 0.15$ 10^6 $M^{-1}s^{-1}$ with 8-oxo-dGTP. See also Supplementary Table S3.

moderately (75.3 ± 3.9 % viable embryos; $P = 0.01$; $n = 150$), whereas injection of 2-OH-dATP did not have any significant effect on viability (97.7 ± 2.3 % viable embryos; $n = 95$). However, if eggs injected with oxidized nucleotides are additionally exposed to 1.5 μmol/L TH588, viability dropped to 6.6 ± 1.3 % for 8-oxo-dGTP ($P = 0.002$; $n = 151$) and 23.4 ± 3.4 % for 2-OH-dATP ($P = 0.009$; $n = 96$; see Fig. 3).

Loss of functional VHL sensitizes to MTH1 inhibition *in vitro* and *in vivo*

Redox signaling networks and hypoxia sensing mechanisms are tightly interwoven in healthy cells, but also work in concert for cancer cells to thrive. The tumor suppressor VHL is involved in hypoxic signaling and patients with a mutated form have a high prevalence for various forms of cancer, especially for clear cell renal carcinomas (33). Using a shRNA approach, we have knocked down VHL in immortalized kidney cells (HAEB) and observed that those cells are more sensitive to MTH1 inhibition compared with controls (see Supplementary Fig. S6). This "VHL disease" is difficult to recapitulate in mice as homozygous VHL knockouts die *in utero* (34). Homozygous knockout zebrafish, however, are viable until 7 days after fertilization (dpf), and are therefore a unique and powerful model system (22) that we used to study if MTH1 inhibition is connected to VHL activity. We morphologically separated homozygous VHL mutants from heterozygous/wild-types at 4 dpf and exposed the groups to 10 μmol/L TH588 (see Fig. 4A and Supplementary Fig. S7). Although treatment of heterozygous or wild-type embryos did not cause any morphologic side effects or mortality (viability 95 ± 7 %; $n = 52$), $VHL^{-/-}$ embryos were significantly sensitized to MTH1 inhibition (viability 10 ± 8 %; $n = 52$; $P = 0.0069$; see Fig. 4B and C). The effect of TH588 on $VHL^{-/-}$ embryos is very rapid with the majority of embryos succumbing 24 hours post exposure (see Fig. 4D).

HIF1α activation renders cells dependent on MTH1

The best-characterized function of VHL is its oxygen tension-dependent regulation of HIF1α stability. Therefore, we investigated the potential link between MTH1 inhibition and the role of VHL in regulating HIF1α. The ectopic activation of HIF1α through loss-of-functional VHL can be recapitulated *in vitro* and *in vivo* by inactivation of prolyl hydroxylases (PHD) using DMOG (22). Treatment of zebrafish embryos with DMOG has been done before and shown to phenocopy VHL mutations as well as to upregulate *bona fide* HIF1α target genes (35). Interestingly, we observed an upregulation of MTH1 in embryos with ectopically activated VHL-Hif1α signaling, indicating a biologic function in this context (see Supplementary Figs. S8 and S9). As shown by van

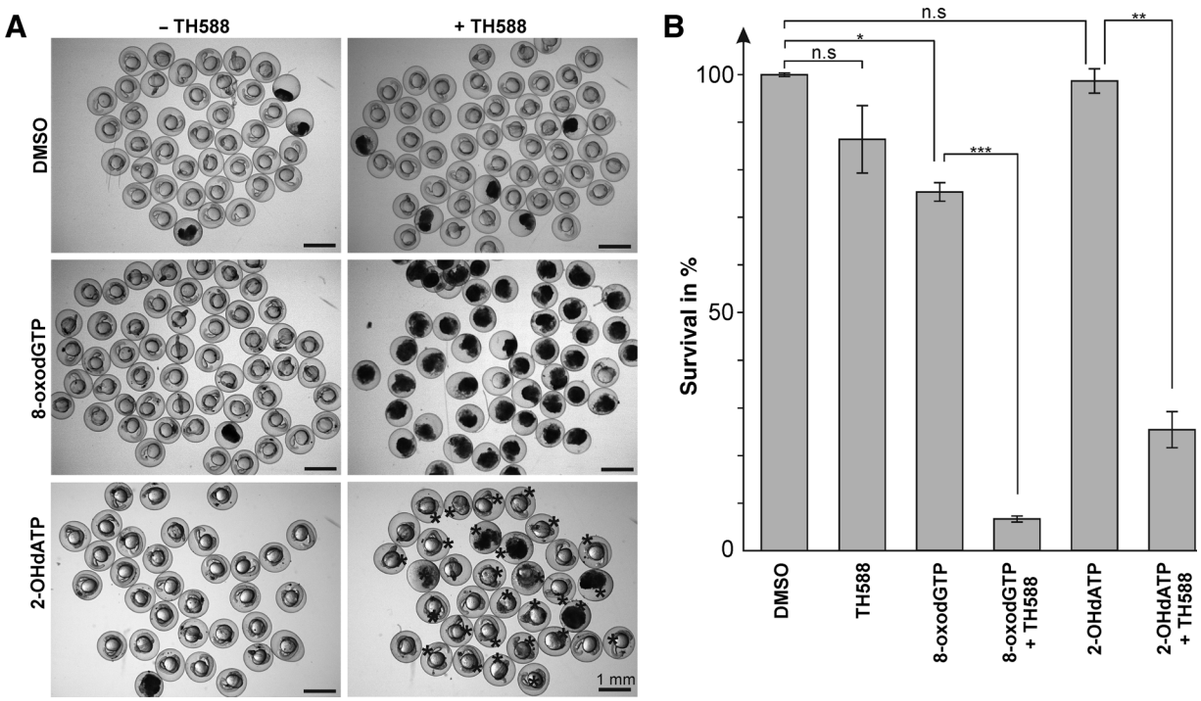

Figure 3.
Injection of oxidized nucleotides into zebrafish eggs. A, of note, 1.5 nL of a 1.3 mmol/L solution of 8-oxo-dGTP or 2-OH-dATP was injected into one cell stage eggs; dead embryos are either black (disintegrated) or marked with an asterisk (cardiac arrest). Survival decreased moderately for embryos injected with 8-oxo-dGTP (75.3 ± 3.9 % viable embryos; *, $P = 0.01$; $n = 150$); injection of 2-OH-dATP did not have a significant effect on embryo survival. Additional exposure to 10 μmol/L TH588 reduced survival to 6.6 ± 1.3 % for 8-oxo-dGTP (***, $P = 0.002$; $n = 151$) and 23.4 ± 3.4 % for 2-OH-dATP (**, $P = 0.009$; $n = 96$). B, embryos with cardiac arrest were regarded as dead. n.s., nonsignificant.

Rooijen and colleagues (22), we also observed that treatment of embryos with DMOG alone did not have any significant effect on survival (viable embryos 100% ± 0%, $n = 50$). However, viability decreased dramatically upon additional exposure to 10 μmol/L TH588 (viable embryos 6.7% ± 9%; $P = 0.005$; $n = 50$). Because it is established that activation of hypoxic signaling induces the formation of reactive oxygen species (ROS) in mitochondria (5), we pretreated DMOG-exposed embryos with the antioxidants NAC or PEG-catalase as well as overexpressed the general antioxidant enzyme Gpx1a. The increase of antioxidant capacity significantly protected against MTH1 inhibition (viable embryos 76% ± 6%; $n = 60$; $P = 0.017$ for NAC pretreatment; 81% ± 7.5%; $n = 54$; $P = 0.0001$ for PEG-catalase treatment and 83% ± 11.7%; $n = 32$; $P = 0.00034$ for zfGprx1 overexpression; see Fig. 5A and B). We have used our ZebROS transgenic line that genetically encodes a previously described *in vivo* sensor probing either the cytosolic or mitochondrial glutathione redox state (29) to assess whether this redox potential changes upon DMOG treatment. We were able to show that the absorbance ratio$_{405/492}$ in ZebROS embryos with the cytosolic sensor increased from 0.019 ± 0.044 for control embryos to 0.026 ± 0.001 upon DMOG treatment for 24 hours ($P = 0.0005$; $n = 46$ per group). Also the 405/492 absorption ratio in the ZebROS harboring the mitochondrial construct increased, from 0.016 ± 0.002 for control embryos to 0.027 ± 0.008 for DMOG-treated embryos ($P = 2 \times 10^{-11}$; $n = 48$ per group), indicating an oxidation of the cytosolic and mitochondrial glutathione pool in DMOG-treated embryos (see Fig. 5C and D; Supplementary Fig. S10).

Discussion

The malignant redox environment is closely interwoven with many oncogenes including RAS, to allow for tumor progression and metastasis (6, 36, 37). However, it is known that this cross-talk leads to an increase of cellular ROS production via overactivation of NADPH oxidases among others (38–40). To counteract the detrimental effects of increased ROS production, cancer cells upregulate defense mechanisms including MTH1 (17). Despite the plastic cellular redox environment, we were able to show that exposing healthy cells to oxidants or depletion of the cellular glutathione pool increased their sensitivity to MTH1 inhibition. This is in accordance with previous observations that exposure to hydrogen peroxide sensitized both fibroblasts and cancer cells to siRNA-mediated knockdown of MTH1 (41). Moreover, we provide evidence that pretreatment of cancer cells with the thiol antioxidant NAC as well as the non-thiol antioxidant PEG-catalase protects against MTH1 inhibition. These data indicate that the cellular redox environment is a key factor in determining sensitivity to MTH1 inhibition. Because radiotherapy induces oxidative stress as well as nucleotide damage and the DNA damage response of cancer cells counteracts this mode of treatment (42), it will be interesting to evaluate MTH1 inhibitors as radio-sensitizers and as cotreatment together with radiotherapy.

The zebrafish is a powerful model for preclinical research, including cancer (43). We found the MTH1 protein to be highly conserved on amino acid level, and determined the crystal structure of zfMTH1 together with our potent and selective MTH1

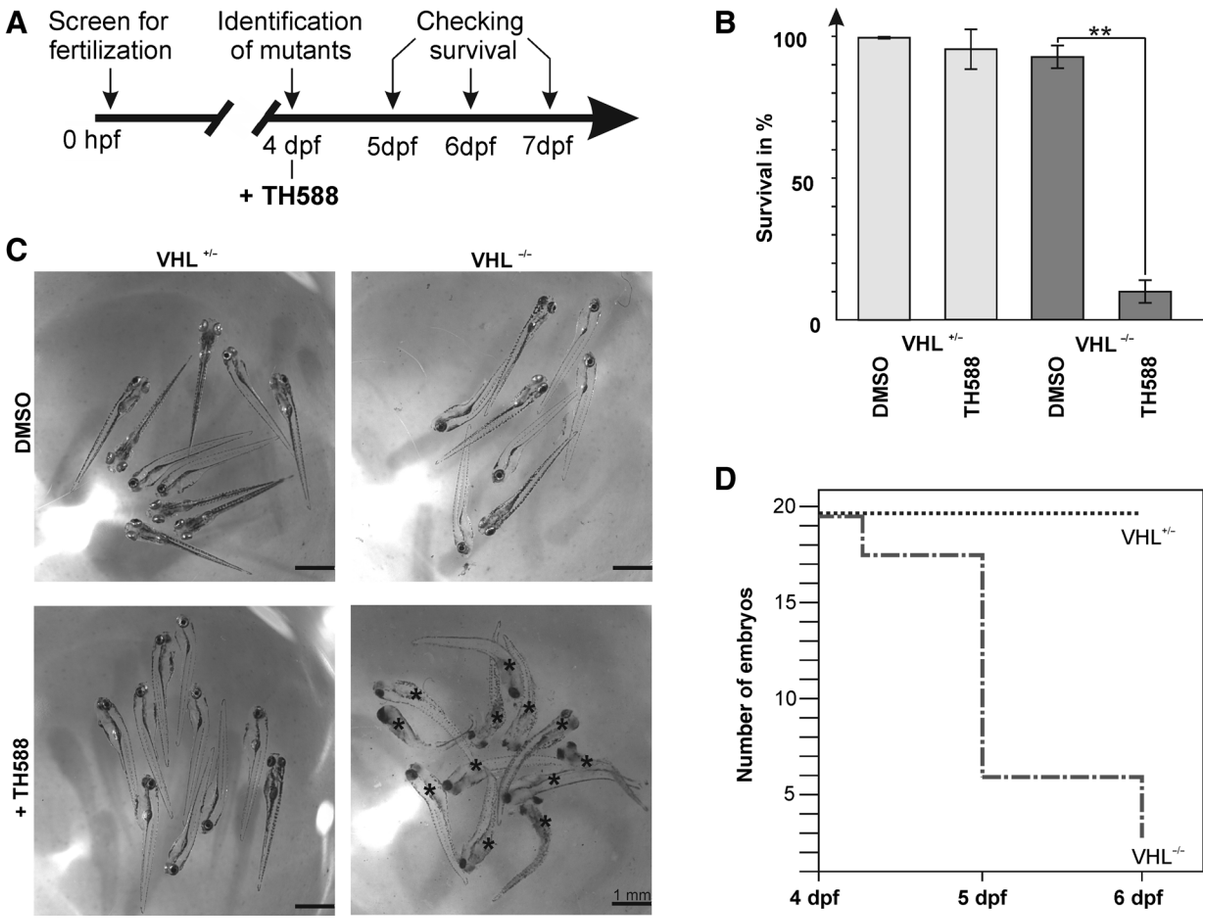

Figure 4.
Loss of functional VHL sensitizes to MTH1 inhibition. Zebrafish embryos mutated for VHL were identified and treated as shown in A. Survival of wild-type/VHL$^{+/-}$ embryos was not affected upon exposure to DMSO (100 $\pm$ 0 %; $n = 52$) or 10 μmol/L TH588 (viability 95 $\pm$ 7 %; $n = 52$). B, survival of VHL$^{-/-}$ embryos exposed to TH588 dropped to 10 $\pm$ 8 %; $n = 52$ compared with 96 $\pm$ 4 % viable control embryos ($n = 52$; **, $P = 0.0069$). C, embryos with cardiac arrest were regarded as dead and are marked with an asterisk. Effect of TH588 treatment on VHL$^{-/-}$ embryos was rapid, with most embryos dying 24 hours after exposure; representative survival curve out of three experiments (D).

inhibitor TH588 (19). Because of significant structural and biochemical similarities of zfMTH1 and hMTH1, and because the hMTH1 inhibitor TH588 tightly binds and efficiently inhibits zfMTH1, the zebrafish is a relevant *in vivo* model to study MTH1 biology. Moreover, oxidized nucleotides can easily be microinjected into the zebrafish eggs and thereby be distributed uniformly throughout the developing embryo. This circumvents the problem that nucleotide triphosphates (dNTP) are not taken up by cells and even with today's best methods, for example, transfection or hypotonic shifts, membrane penetration is inconsistent and difficult to quantify. Utilizing this model, we provide *in vivo* evidence that 8-oxo-dGTP and 2-OH-dATP are indeed toxic to zebrafish in absence of MTH1 activity. The high toxicity of the oxidized nucleotides was surprising, as despite the high mutagenic potential of 8-oxodG in DNA, the lesion is generally regarded as nontoxic to the organism because the replication fork remains intact at those sites and the respective repair enzymes are nonessential (31, 31). We cannot exclude that the injected oxidized nucleotides are incorporated into RNA to generate toxic lesions; however, to our knowledge, there is no biochemical pathway that converts 8-oxo-dGTP to 8-oxoGTP and that could explain the fast death of the embryos. We are currently elucidating the molecular mechanism to bring more light into this interesting observation.

Cancer cells are not only characterized by an oncogenic redox environment but also by deregulation of the VHL-HIF1α hypoxia signaling axis (33). Loss-of-functional VHL (and therefore stabilization of HIF1α) predisposes to various malignancies (44) and overexpression/overactivation of HIF1α is correlated with poor prognosis in a number of cancers (45). In zebrafish, we observed this deregulation to be accompanied by MTH1 upregulation, indicating an important function for this nononcogenic addition enzyme in this context. Indeed, we have found that loss of VHL and/or chemically induced overactivation of HIF1α signaling sensitizes to MTH1 inhibition *in vivo*. Interestingly, it has been described that hypoxia induces the formation of ROS at complex III of the mitochondrial electron transport chain, leading to a more oxidized cellular and mitochondrial environment, and the activation of hypoxia signaling (46–48). Real-time measurement of the glutathione potential *in vivo* in drosophila has been proven

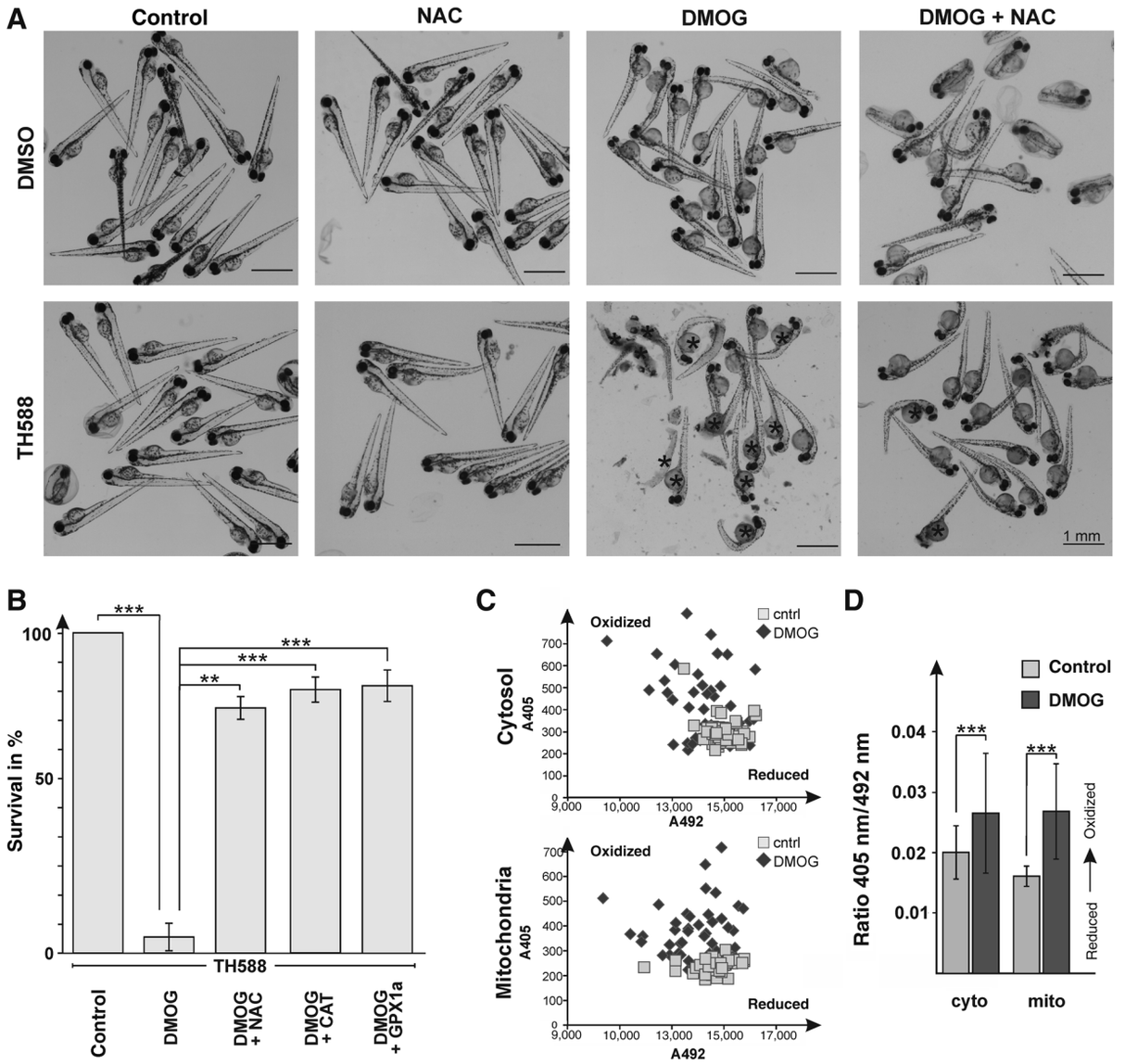

Figure 5.
Activation of HIF1α oxidizes the cellular glutathione pool and sensitizes to MTH1 inhibition. A and B, treatment of embryos with 10 TH588 and 75 μmol/L DMOG decreased survival to 5 ± 7 % ($P = 0.0003$) compared with controls. If embryos exposed to DMOG were pretreated with 10 mmol/L NAC for 2 hours before TH588 addition, the embryos survival was significantly improved (viability of 76% ± 6%; $n = 60$; $P = 0.017$). B, besides NAC, we exposed DMOG-treated embryos also to the antioxidants PEG-Catalase or zfGpx1a and restored survival to 81% ± 8%; $n = 54$ ($P = 0.0001$) and 83% ± 12%; $n = 32$ ($P = 0.00034$), respectively. We used ZebROS embryos harboring a genetically encoded probe to measure the cytosolic and mitochondrial redox potential. DMOG exposure increased in the cytosolic ZebROS embryos the absorbance 405/492 ratio from 0.019 ± 0.044 for control embryos to 0.026 ± 0.001 for DMOG embryos ($P = 0.0005$; $n = 46$ per group). C and D, also the 405/492 absorption ratio in the mitochondrial ZebROS increased, from 0.016 ± 0.002 for control embryos to 0.027 ± 0.008 for DMOG embryos ($P = 2 \times 10^{-11}$; $n = 48$ per group), indicating a more oxidized cytosolic and mitochondrial glutathione pool in DMOG-treated embryos.

powerful (49), and therefore we developed transgenic zebrafish that genetically encodes the same glutathione sensor. We observed in line with the literature that ZebROS embryos had a more oxidized redox state of the glutathione pool after mimicking hypoxic conditions by DMOG treatment. Because preexposure or overexpression of antioxidants in embryos protected against MTH1 inhibitor induced death, elevated redox pressure in embryos with deregulated VHL-HIF1α signaling might be the underlying cause for the sensitization to MTH1 inhibition (see Fig. 6).

With this work we have provided evidence that the oncogenic cellular redox system is a critical factor determining sensitivity to MTH1 inhibition. As most cancers are characterized by increased oxidative pressure and/or a deregulated VHL-HIF1α axis, MTH1 inhibition could potentially target many different cancer indications, even those that have a poor prognosis today. Importantly,

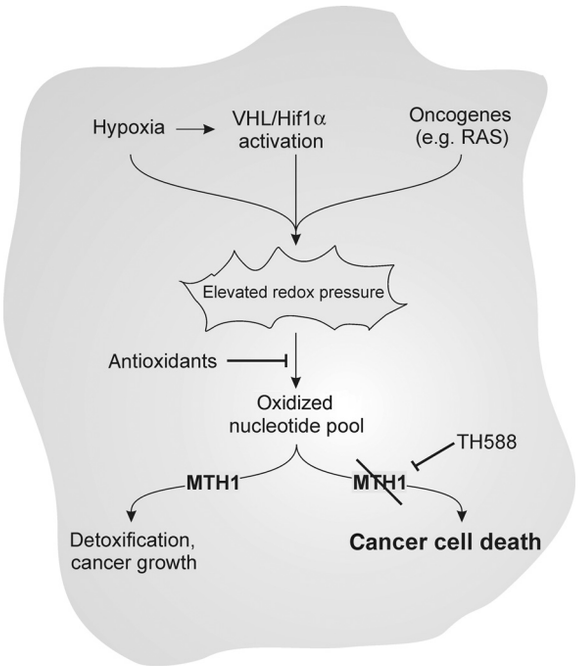

Figure 6.
Elevated redox pressure sensitizes cancer cells to MTH1 inhibition. Cancer cells suffer from elevated redox pressure, for example, due to hypoxic conditions, deregulated hypoxia signaling, or oncogene expression. This cancer cell-specific redox environment leads to a more oxidized nucleotide pool, which requires the enzymatic activity of MTH1 for sanitation. If MTH1 is inhibited, oxidized nucleotides can cause DNA damage and eventually lead to cancer cell death (19).

not only tumors are characterized by a specific, more oxidized redox system, but also other major health issues including neurodegeneration (50, 51) and rheumatoid arthritis (52). It will be interesting to investigate whether MTH1 plays a critical role in these diseases as well.

Disclosure of Potential Conflicts of Interest

T. Helleday has ownership interest in a patent on MTH1 inhibitors. No potential conflicts of interest were disclosed by the other authors.

Authors' Contributions

Conception and design: L. Bräutigam, A.-S. Jemth, U. Warpman Berglund, P. Stenmark, T. Helleday
Development of methodology: L. Bräutigam, A.-S. Jemth
Acquisition of data (provided animals, acquired and managed patients, provided facilities, etc.): L. Bräutigam, L. Pudelko, A.-S. Jemth, H. Gad, M. Narwal, R. Gustafsson, S. Karsten, J. Carreras Puigvert
Analysis and interpretation of data (e.g., statistical analysis, biostatistics, computational analysis): L. Bräutigam, L. Pudelko, A.-S. Jemth, H. Gad, M. Narwal, R. Gustafsson, E. Homan, C. Berndt, P. Stenmark, T. Helleday
Writing, review, and/or revision of the manuscript: L. Bräutigam, A.-S. Jemth, H. Gad, M. Narwal, R. Gustafsson, E. Homan, C. Berndt, U. Warpman Berglund, P. Stenmark, T. Helleday
Administrative, technical, or material support (i.e., reporting or organizing data, constructing databases): L. Bräutigam
Study supervision: L. Bräutigam, U. Warpman Berglund, P. Stenmark, T. Helleday

Acknowledgments

The authors thank the staff of the zebrafish core facility at Karolinska Institutet for excellent service, Kristina Edfelt and Linn Yngvesson for administrative assistance, Sabina Eriksson for laboratory assistance and Tobias Koolmeister and Martin Henriksson for synthesis of TH588. Furthermore, the Protein Expression and Characterization facility at Scilifelab for help with protein purification and the beamline scientists at BESSY, Germany; ESRF, France; Max-Lab, Sweden and the Swiss Light Source, Switzerland for their support in structural biology data collection and Biostruct-X for support. The authors also thank that Tobias Dick (DKFZ) provided the GSH sensor plasmids within a collaboration established in the priority program 1710 of the Deutsche Forschungsgemeinschaft and Dr. William Hahn (Dana-Farber Cancer Institute, Boston, MA) for providing the BJ-hTERT cells.

Grant Support

This work was supported by the Swedish society for medical research (L. Bräutigam), the Karolinska Institutes KID funding (L. Pudelko), the Deutsche Forschungsgemeinschaft (C. Berndt), and the Knut and Alice Wallenberg Foundation (T. Helleday and P. Stenmark), the Swedish Foundation for Strategic Research (T. Helleday and P. Stenmark), the Swedish Cancer Society (T. Helleday and P. Stenmark), the Swedish Research Council (T. Helleday and P. Stenmark), the Wenner-Gren Foundation (P. Stenmark), and the Göran Gustafsson Foundation, the Swedish Children's Cancer Foundation, the Swedish Pain Relief Foundation, and the Torsten and Ragnar Söderberg Foundation (T. Helleday).

The costs of publication of this article were defrayed in part by the payment of page charges. This article must therefore be hereby marked *advertisement* in accordance with 18 U.S.C. Section 1734 solely to indicate this fact.

Received September 8, 2015; revised January 26, 2016; accepted January 29, 2016; published OnlineFirst February 9, 2016.

References

1. Holmström KM, Finkel T. Cellular mechanisms and physiological consequences of redox-dependent signalling. Nat Rev Mol Cell Biol 2014;15:411–21.
2. Zhang Y, Du Y, Le W, Wang K, Kieffer N, Zhang J. Redox control of the survival of healthy and diseased cells. Antioxid Redox Signal 2011;15:2867–908.
3. Szatrowski TP, Nathan CF. Production of large amounts of hydrogen peroxide by human tumor cells. Cancer Res 1991;51:794–98.
4. Gius D, Spitz DR. Redox signaling in cancer biology. Antioxid Redox Signal 2006;8:1249–52.
5. Hielscher A, Gerecht S. Hypoxia and free radicals: role in tumor progression and the use of engineering-based platforms to address these relationships. Free Radic Biol Med 2015;79:281–91.
6. Heo J. Redox control of GTPases: from molecular mechanisms to functional significance in health and disease. Antioxid Redox Signal 2011;14:689–724.
7. Moon EJ, Giaccia A. Dual roles of NRF2 in tumor prevention and progression: possible implications in cancer treatment. Free Radic Biol Med 2015;79:292–9.
8. Noble M, Mayer-Pröschel M, Li Z, Dong T, Cui W, Pröschel C, et al. Redox biology in normal cells and cancer: restoring function of the redox/Fyn/c-Cbl pathway in cancer cells offers new approaches to cancer treatment. Free Radic Biol Med 2015;79:300–23.
9. Trachootham D, Alexandre J, Huang P. Targeting cancer cells by ROS-mediated mechanisms: a radical therapeutic approach? Nat Rev Drug Discov 2009;8:579–91.
10. Sabharwal SS, Schumacker PT. Mitochondrial ROS in cancer: initiators, amplifiers or an Achilles' heel? Nat Rev Cancer 2014;14:709–21.
11. Adams DJ, Boskovic ZV, Theriault JR, Wang AJ, Stern AM, Wagner BK, et al. Discovery of small-molecule enhancers of reactive oxygen species that are nontoxic or cause genotype-selective cell death. ACS Chem Biol 2013;8:923–29.

12. Haghdoost S, Sjölander L, Czene S, Harms-Ringdahl M. The nucleotide pool is a significant target for oxidative stress. Free Radic Biol Med 2006;41:620–6.
13. Sakumi K, Furuichi M, Tsuzuki T, Kakuma T, Kawabata S, Maki H, et al. Cloning and expression of cDNA for a human enzyme that hydrolyzes 8-oxo-dGTP, a mutagenic substrate for DNA synthesis. J Biol Chem 1993; 268:23524–30.
14. Oka S, Ohno M, Tsuchimoto D, Sakumi K, Furuichi M, Nakabeppu Y. Two distinct pathways of cell death triggered by oxidative damage to nuclear and mitochondrial DNAs. EMBO J 2008;27:421–32.
15. Ichikawa J, Tsuchimoto D, Oka S, Ohno M, Furuichi M, Sakumi K, et al. Oxidation of mitochondrial deoxynucleotide pools by exposure to sodium nitroprusside induces cell death. DNA Repair 2008;7:418–30.
16. Fujikawa K, Kamiya H, Yakushiji H, Nakabeppu Y, Kasai H. Human MTH1 protein hydrolyzes the oxidized ribonucleotide, 2-hydroxy-ATP. Nucleic Acids Res 2001;29:449–54.
17. Rai P. Human Mut T Homolog 1 (MTH1): a roadblock for the tumor-suppressive effects of oncogenic RAS-induced ROS. Small GTPases 2012; 3:120–5.
18. Rai P, Young JJ, Burton DGA, Giribaldi MG, Onder TT, Weinberg RA. Enhanced elimination of oxidized guanine nucleotides inhibits oncogenic RAS-induced DNA damage and premature senescence. Oncogene 2011; 30:1489–96.
19. Gad H, Koolmeister T, Jemth A-S, Eshtad S, Jacques SA, Ström CE, et al. MTH1 inhibition eradicates cancer by preventing sanitation of the dNTP pool. Nature 2014;508:215–21.
20. Huber KVM, Salah E, Radic B, Gridling M, Elkins JM, Stukalov A, et al. Stereospecific targeting of MTH1 by (S)-crizotinib as an anticancer strategy. Nature 2014;508:222–7.
21. McCurley AT, Callard GV. Characterization of housekeeping genes in zebrafish: male-female differences and effects of tissue type, developmental stage and chemical treatment. BMC Mol Biol 2008;9:102.
22. van Rooijen E, Voest EE, Logister I, Korving J, Schwerte T, Schulte-Merker S, et al. Zebrafish mutants in the von Hippel-Lindau tumor suppressor display a hypoxic response and recapitulate key aspects of Chuvash polycythemia. Blood 2009;113:6449–60.
23. Kabsch W. XDS. Acta Crystallogr D Biol Crystallogr 2010;66:125–32.
24. Adams DJ, Boskovic ZV, Theriault JR, Wang AJ, Stern AM, Wagner BK, et al. PHENIX: a comprehensive Python-based system for macromolecular structure solution. Acta Crystallogr D Biol Crystallogr 2010;66:213–21.
25. Svensson LM, Jemth A-S, Desroses M, Loseva O, Helleday T, Högbom M, et al. Crystal structure of human MTH1 and the 8-oxo-dGMP product complex. FEBS Lett 2011;585:2617–21.
26. Murshudov GN, Vagin AA, Dodson EJ. Refinement of macromolecular structures by the maximum-likelihood method. Acta Crystallogr D Biol Crystallogr 1997;53:240–55.
27. Emsley P, Cowtan K. Coot: model-building tools for molecular graphics. Acta Crystallogr D Biol Crystallogr 2004;60:2126–32.
28. Suster ML, Kikuta H, Urasaki A, Asakawa K, Kawakami K. Transgenesis in zebrafish with the tol2 transposon system. Methods Mol Biol Clifton NJ 2009;561:41–63.
29. Gutscher M, Pauleau A-L, Marty L, Brach T, Wabnitz GH, Samstag Y, et al. Real-time imaging of the intracellular glutathione redox potential. Nat Methods 2008;5:553–9.
30. Sakumi K, Tominaga Y, Furuichi M, Xu P, Tsuzuki T, Sekiguchi M, et al. Ogg1 knockout-associated lung tumorigenesis and its suppression by Mth1 gene disruption. Cancer Res 2003;63:902–5.
31. Tsuzuki T, Egashira A, Igarashi H, Iwakuma T, Nakatsuru Y, Tominaga Y, et al. Spontaneous tumorigenesis in mice defective in the MTH1 gene encoding 8-oxo-dGTPase. Proc Natl Acad Sci U S A 2001;98:11456–61.
32. Dominissini D, He C. Cancer: damage prevention targeted. Nature 2014; 508:191–2.
33. Gossage L, Eisen T, Maher ER. VHL, the story of a tumour suppressor gene. Nat Rev Cancer 2015;15:55–64.
34. Haase VH. The VHL tumor suppressor in development and disease: functional studies in mice by conditional gene targeting. Semin Cell Dev Biol 2005;16:564–74.
35. Metelo AM, Noonan HR, Li X, Jin Y, Baker R, Kamentsky L, et al. Pharmacological HIF2α inhibition improves VHL disease-associated phenotypes in zebrafish model. J Clin Invest 2015;125: 1987–97.
36. Finkel T. Intracellular redox regulation by the family of small GTPases. Antioxid Redox Signal 2006;8:1857–63.
37. Mitchell L, Hobbs GA, Aghajanian A, Campbell SL. Redox regulation of Ras and Rho GTPases: mechanism and function. Antioxid Redox Signal 2013;18:250–8.
38. Block K, Gorin Y. Aiding and abetting roles of NOX oxidases in cellular transformation. Nat Rev Cancer 2012;12:627–37.
39. Irani K, Xia Y, Zweier JL, Sollott SJ, Der CJ, Fearon ER, et al. Mitogenic signaling mediated by oxidants in Ras-transformed fibroblasts. Science 1997;275:1649–52.
40. Lee AC, Fenster BE, Ito H, Takeda K, Bae NS, Hirai T, et al. Ras proteins induce senescence by altering the intracellular levels of reactive oxygen species. J Biol Chem 1999;274:7936–40.
41. Youn C-K, Jun JY, Hyun J-W, Hwang G, Lee BR, Chung MH, et al. hMTH1 depletion promotes oxidative-stress-induced apoptosis through a Noxa- and caspase-3/7-mediated signaling pathway. DNA Repair 2008;7:1809–23.
42. Tian H, Gao Z, Li H, Zhang B, Wang G, Zhang Q, et al. DNA damage response–a double-edged sword in cancer prevention and cancer therapy. Cancer Lett 2015;358:8–16.
43. White R, Rose K, Zon L. Zebrafish cancer: the state of the art and the path forward. Nat Rev Cancer 2013;13:624–36.
44. Robinson CM, Ohh M. The multifaceted von Hippel-Lindau tumour suppressor protein. FEBS Lett 2014;588:2704–11.
45. Semenza GL. Hypoxia-inducible factors in physiology and medicine. Cell 2012;148:399–408.
46. Chandel NS, McClintock DS, Feliciano CE, Wood TM, Melendez JA, Rodriguez AM, et al. Reactive oxygen species generated at mitochondrial complex III stabilize hypoxia-inducible factor-1alpha during hypoxia: a mechanism of O2 sensing. J Biol Chem 2000;275:25130–8.
47. Chandel NS, Maltepe E, Goldwasser E, Mathieu CE, Simon MC, Schumacker PT. Mitochondrial reactive oxygen species trigger hypoxia-induced transcription. Proc Natl Acad Sci U S A 1998;95:11715–20.
48. Peng Y-J, Yuan G, Ramakrishnan D, Sharma SD, Bosch-Marce M, Kumar GK, et al. Heterozygous HIF-1alpha deficiency impairs carotid body-mediated systemic responses and reactive oxygen species generation in mice exposed to intermittent hypoxia. J Physiol 2006; 577:705–16.
49. Albrecht SC, Barata AG, Großhans J, Teleman AA, Dick TP. *In vivo* mapping of hydrogen peroxide and oxidized glutathione reveals chemical and regional specificity of redox homeostasis. Cell Metab 2011;14:819–29.
50. von Bernhardi R, Eugenín J. Alzheimer's disease: redox dysregulation as a common denominator for diverse pathogenic mechanisms. Antioxid Redox Signal 2012;16:974–1031.
51. Dias V, Junn E, Mouradian MM. The role of oxidative stress in Parkinson's disease. J Park Dis 2013;3:461–91.
52. Chiurchiù V, Maccarrone M. Chronic inflammatory disorders and their redox control: from molecular mechanisms to therapeutic opportunities. Antioxid Redox Signal 2011;15:2605–41.